Catalysis Today 142 (2009) 320–328

Contents lists available at ScienceDirect

Catalysis Today

journal homepage: www.elsevier.com/locate/cattod

The effect of Nb or Ta substitution into the M1 phase of the MoV(Nb,Ta)TeO selective oxidation catalyst

William D. Pyrz [a], Douglas A. Blom [b], N. Raveendran Shiju [c], Vadim V. Guliants [c], Thomas Vogt [d], Douglas J. Buttrey [a,*]

[a] Center for Catalytic Science and Technology, Department of Chemical Engineering, University of Delaware, Colburn Laboratory, 150 Academy Street, Newark, DE 19716, United States
[b] NanoCenter and Electron Microscopy Center, University of South Carolina, Columbia, SC 29208, United States
[c] Department of Chemical and Materials Engineering, University of Cincinnati, Cincinnati, OH 45221, United States
[d] NanoCenter and Department of Chemistry and Biochemistry, University of South Carolina, Columbia, SC 29208, United States

ARTICLE INFO

Article history:
Available online 24 December 2008

Keywords:
Aberration-corrected STEM
HAADF
M1/M2
MoVTeNbO
MoVTaTeO
Propane oxidation

ABSTRACT

We use aberration corrected high-angle annular dark field (HAADF) imaging to systematically study, atomic column by atomic column, the effects of substituting Nb or Ta into the M1 phase of the MoV(Nb,Ta)TeO propane (amm)oxidation catalyst. The HAADF results indicate that the *x,y* coordinates of the metal sites within the M1 framework are unaffected by the substitution of either Nb or Ta for Mo. The HAADF analysis of the Ta-substituted catalyst demonstrated that the Ta preferentially substitutes into the pentagonal bipyramidal site, and by analogy, we anticipate that Nb substitutes similarly. Compositional analysis of the entire framework suggests that Ta/Nb behaves as a director of V among the octahedra that link the pentagonal rings, and the variable V occupancy may be correlated with variations in catalytic activities and selectivities. Finally, HAADF imaging provided evidence of coexistence of Ta-rich and Ta-poor domains. Similar phase segregation behavior may be present in Nb-substituted specimens, but would be very difficult to detect.

1. Introduction

Due to the cost differential between propene and propane, the former being derived from crude oil and the latter from natural gas sources, development of processes in which paraffin feeds replace existing olefin feeds are highly desirable. Of relevance to the current study, development and commercialization of selective oxidation and ammoxidation catalysts to make acrylic acid and acrylonitrile, respectively, from propane has significant economic value. At present, the best candidate for the (amm)oxidation of propane involves two-phase synergistic interplay of quinternary oxides in the Mo–V–Nb–Te–O system, with both mixed site occupancies and valences [1–22]. The two phases on which this catalyst system is based were initially identified in a patent by the Mitsubishi Chemical Company and have come to be identified as "M1" and "M2" [17,18,20]. M1 is the majority phase and has an orthorhombic molybdenum bronze structure. Similar to the frameworks of Mo_5O_{14} and $Mo_{17}O_{47}$, the M1 phase is built from center-occupied pentagonal rings that are linked together by corner-sharing octahedral sites (Fig. 1) [6,7].

The arrangement of these linkages is such that hexagonal and heptagonal open channels are present, which can be vacant or occupied by intercalated species. The M1 phase can be described with the generic formula $\{TeO\}_{1-x}\cdot(Mo,V,Nb)_{10}O_{28}$, where the {TeO} moieties are intercalated in hexagonal (and also sometimes heptagonal) channels of the framework [7,22,23]. Based on diffraction data, vanadium is found to predominantly occupy the octahedral sites that link the pentagonal rings, and it has been *assumed* that the Nb occupancy is essentially restricted to the pentagonal centers [6,7,22]. One purpose of this paper is to examine the validity of this assumption.

Motivated by the initial success of the M1/M2 catalyst, the focus of a significant number of studies has since been directed at improving the existing four-component formulation through variations in the M1 composition [3,4,8,24–38], phase fractions split between M1 and M2 [10,14], or the substitution or removal of framework elements [3,4,8,24–38]. Examples of these structural variations include the exclusion of Te and/or Nb (MoVO, MoVTeO) [38,39], using Sb in place of Te (MoVSbO and MoVNbSbO) [3,4,24–26,29,30,33,38], substitution of Nb by Ta (MoVTaTeO) [8,10], or

* Corresponding author. Tel.: +1 302 831 2034; fax: +1 302 831 2085.
E-mail address: dbuttrey@udel.edu (D.J. Buttrey).

0920-5861/$ – see front matter © 2008 Elsevier B.V. All rights reserved.
doi:10.1016/j.cattod.2008.10.051

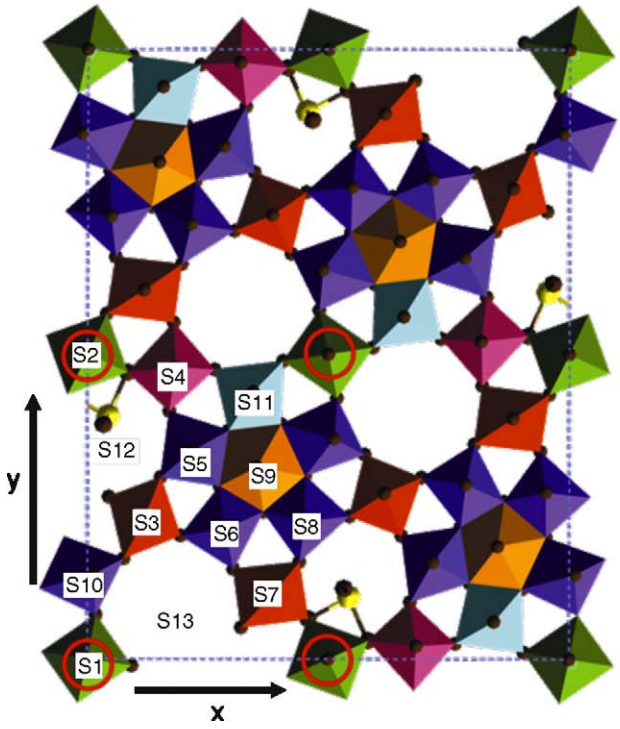

Site	Mo-V-Te-Nb-O Refined Occupancies	Mo-V-Te-Ta-O Refined Occupancies
S1	74% Mo--26% V	100% Mo
S2	38% Mo--62% V	37% Mo--63% V
S3	58% Mo--42% V	34% Mo--64% V
S4	100% Mo	100% Mo
S5	100% Mo	100% Mo
S6	100% Mo	100% Mo
S7	68% Mo--32% V	59%Mo--41%V
S8	100% Mo	100% Mo
S9	100% Nb	56% Mo--44% Ta
S10	100% Mo	100% Mo
S11	100% Mo	100% Mo
S12	74% Te--26% Vacant	67% Te--33% Vacant
S13	20% Te--80% Vacant	18% Te*--82% Vacant
* The refinement yielded unreasonable Te-O distances		

Fig. 1. The atomic framework for the orthorhombic M1 phase with distinct metal sites labeled. The table lists the refined occupancies for the MoVTeNbO [7] and the MoVTeTaO [8] catalyst. A full structural model listing the *x*,*y* coordinates, site occupancies, and atomic positions for oxygen developed by simultaneously refining powder X-ray and neutron data proposed by DeSanto et al. can be found for the MoVTeNbO catalyst in Ref. [7] and the MoVTeTaO catalyst in Ref. [8]. A detailed HR-STEM study providing slight adjustments to the Mo/V occupancy in site S4 can be found in Ref. [22]. The red circles indicate the four different fixed reference points used for assessment of the fractional atomic coordinates.

intercalation of Bi and Cs into the hexagonal and heptagonal channels, respectively [31,40]. Variations in the framework composition lead to catalysts with a substantial range of activities and selectivities for the (amm)oxidation of propane [10,14,15,30,38].

In this report, we directly interpret atomic resolution images acquired from an aberration-corrected JEOL2100F TEM operated in the scanning transmission electron microscope (STEM) mode to systematically evaluate (site-by-site) the variations in the atomic coordinates and atomic column occupancies in the M1 structure. The favorable projection along a ⟨0 0 1⟩ direction, in which the crystallographically inequivalent metal sites do not overlap, permits us to extract elemental occupancies directly from Z-contrast STEM images [22,23]. The goal is to extract meaningful correlations between catalytic activity/selectivity and the composition of the M1 framework. Using these relationships, a better understanding of the catalytic mechanism for propane (amm)oxidation can be developed.

Analysis of microscopic single crystals by TEM eliminates interference from trace impurities that can compromise bulk techniques in the study of multicomponent complex oxides [7,15]. The enhanced resolution provided by aberration-corrected microscopes has been demonstrated in several structural studies, with some examples including the observation of single fullerene (C_{60}) molecules attached to carbon nanotubes, and sub-Ångstrom direct imaging of single gold atoms and dimers [41,42]. For systems closely related to M1, HAADF STEM was used to image the occupancy of Cs ions in the channels of $Cs_{0.5}[Nb_{2.5}W_{2.5}O_{14}]$ [31]. Recently, we have closely studied the orthorhombic M1 structure of the four-component MoVTeNbO catalyst prepared using two different synthetic procedures [23]. These results demonstrated the sensitivity of the composition of the M1 phase to synthetic conditions. The sample prepared using slurry methods exhibited Te filling in both the heptagonal and hexagonal channels, whereas the hydrothermal method only showed Te in the hexagonal channels [23]. Furthermore, subtle variations in the contrast of mixed Mo/V atomic columns suggested further compositional differences between the two catalysts [23].

In this study, we report on the effect of Group V transition element substitution on the M1 framework structure. The high Z of Ta, as a site-specific substitution for Nb, provides us with an indirect probe to test the proposed location of Nb in the M1 framework; Ta is chemically very similar to Nb, being isoelectronic, of similar radius, and forming similar compounds. Nb is indistinguishable from Mo using standard X-ray or electron methods; in the present case with Nb^{5+} and Mo^{6+}, we have isoelectronic species with nearly identical radii such that the form factors are very closely matched [7]. Usually, such problems with X-ray and electron contrast from similar or isoelectronic elements are overcome by using neutron diffraction, for which the nuclear scattering mechanism is isotope-dependent. In this instance, however, ^{93}Nb and the natural mix of Mo isotopes (^{92}Mo–^{100}Mo) leave us with insufficient contrast differences, since the coherent neutron scattering cross-section for Nb is 6.23 barns, as compared with 5.80 barns weighted average for natural Mo [43]. Substitution of Nb by Ta provides significant contrast for both electron and X-ray approaches. In an earlier study, the structural consequences of Ta substitution for Nb were explored by simultaneous Rietveld refinement of X-ray and neutron data [8]. In this study, we use the differences in electron scattering cross-section, including specimens substituted with Ta, to characterize coordinates and occupancies in individual atomic columns by HAADF imaging, and we compare with the prior Rietveld results. In doing so, we will also make

comparisons of the three-component MoVTeO with the four-component MoVNbTeO and MoVTaTeO catalysts.

2. Experimental methods

2.1. Catalyst preparation

Two different synthetic approaches were used for the synthesis of the M1 specimens examined in this study. The Ta-substituted M1 phase was prepared using previously published slurry methods [8] at ambient pressure and yielded nearly phase pure M1. This sample was the same as that used for the structure refinement described by DeSanto et al. [8a] for MoVTeTaO and will be referred to as M1-Ta. The last two M1 catalysts were made using hydrothermal synthesis, combining appropriate amounts of ammonium heptamolybdate hydrate ($(NH_4)_6[Mo_7O_{24}]\cdot 4H_2O$), vanadyl sulfate ($VOSO_4$), niobium oxalate ($Nb(HC_2O_4)_5\cdot 6H_2O$), and tellurium oxide ($TeO_2$) at 175 °C for 48 h or 72 h under autogenous pressure (~8.9 bar) to yield either the MoVTeO or MoVTeNbO, respectively. After the synthesis, the solid product was filtered, washed several times with de-ionized water, and dried at 80 °C overnight. The products were then calcined in a flow of ultra-pure N_2 at 873 K (MoVTeNbO) or 773 K (MoVTeO). All samples presented in this study were fresh catalysts characterized after calcination. These samples will be referred to as M1-Mo and M1-Nb for the MoVTeO and MoVNbTeO samples, respectively. Table 1 provides the sample ID, the nominal synthetic composition and preparation procedure, previous catalytic results, and the associated references providing catalytic details.

2.2. Electron microscopy

Aberration-corrected HR-STEM was used to image the materials with a JEOL 2100F equipped with a CEOS C_s-corrector on the illumination system at the Electron Microscopy Center of the University of South Carolina. The geometrical aberrations were measured and controlled to provide less than a $\pi/4$ phase shift of the incoming electron waves over the probe-defining aperture of 14.5 mrad or 15.4 mrad. HAADF STEM images were acquired on a Fischione Model 3000 HAADF detector with a camera length such that the inner cut-off angle of the detector was at least 65.6 mrad. The scanning acquisition was synchronized to the 60 Hz AC electrical power to minimize 60 Hz noise in the images and a pixel dwell time range between 7 μs and 32 μs was selected. Each sample was prepared for STEM by finely grinding the as-prepared catalyst specimen and then dipping a holey-carbon coated Cu grid into the powder.

2.3. Micrograph analysis/interpretation

2.3.1. Metal site coordinates

Because the M1 structure has no overlapping crystallographically distinct metal sites in the ⟨0 0 1⟩ projections, direct extraction of fractional *x* and *y* atomic coordinates is possible. These coordinates were determined by placing an adjustable grid across the unit cell. This adjustable grid was necessary to compensate for the rastering and sample drift distortions. To minimize the influence of these distortions, each metal coordinate site within the first quadrant of a chosen unit cell was measured and averaged for four different reference points [(0,0), (0,0.5), (0.5,0), (0.5,0.5)], corresponding to projections of the binary axes for *Pba*2 (Space Group No. 32) [44] symmetry; these are labeled in Fig. 1 (red circles). By using four reference points fixed by symmetry, we effectively cut in half the maximum distance that any given atomic column lies from the nearest point of reference. By sampling with respect to each of the four nearest reference points, the systematic errors due to the rastering distortions and environmental disturbances cancel (ideal case) and the average of the measured fractional *x*,*y* coordinate best reflects the true atomic position within the unit cell.

2.3.2. Metal site occupancies

We made the following assumptions when calculating the site occupancies and comparing HAADF–STEM contrast levels between different crystallites: (1) the observed intensities follow the Z^2 Rutherford scattering relationship [45,46], (2) within a unit cell, the thickness of the crystal was assumed constant, (3) scattering contributions from oxygen were only considered at positions superimposed in the ⟨0 0 1⟩ projections with the metal site columns, (4) a constant integration area was appropriate for all metal framework sites, and (5) the background was constant throughout the unit cell. Using these assumptions, the total intensity for each atomic column was calculated by integrating the individual pixel intensity for each framework site. The background from several empty heptagonal channels in the vicinity of the unit cell of interest was averaged and then subtracted from the integrated intensity of each site. The contrast ratio shown in several figures below was calculated by taking the raw intensities after background subtraction and was normalized by the average intensity of the five octahedral members of the pentagonal ring. This normalization approach was used because we expect the occupancy of pentagonal ring octahedral sites to be at or very close to 100% Mo based on the prior refinements of the MoVTeNbO and MoVTeTaO M1 phases [7,8]. This normalization procedure allows direct comparison of the occupancy of all other sites using the contrast ratio, and variations within the pentagonal ring octahedra can be examined as a test of the normalization assumption.

3. Results and discussions

3.1. Qualitative structural analysis

Isolated, thin crystallites from the M1-Mo, M1-Nb, and M1-Ta specimens were oriented for ⟨0 0 1⟩ zone observation. A representative image for each of the three catalysts is shown in Fig. 2, where the a and b axes are indicated. In all three images, the atomic columns are well-resolved and exhibit the expected orthorhombic framework (Fig. 1). Furthermore, there are clear contrast variations among the atomic columns throughout the image reflecting occupancy differences across the framework structure. Contrast

Table 1
Table listing the sample ID, nominal synthesis composition, preparation technique, catalytic yield for acrylonitrile, and references providing complete catalytic information.

Catalyst performance, composition, and synthetic methods for MoVTe(Nb,Ta)O				
ID	Nominal metal composition	Preparation method	Acrylonitrile yields (%)	Reference
M1-Mo	$Mo_{1.00}V_{0.49}Te_{0.17}$	Hydrothermal	8	[48]
M1-Nb	$Mo_{1.00}V_{0.31}Nb_{0.14}Te_{0.27}$	Precursor slurry	43	[7,10]
M1-Ta	$Mo_{1.00}V_{0.31}Ta_{0.10}Te_{0.22}$	Precursor slurry	41	[8a,10]

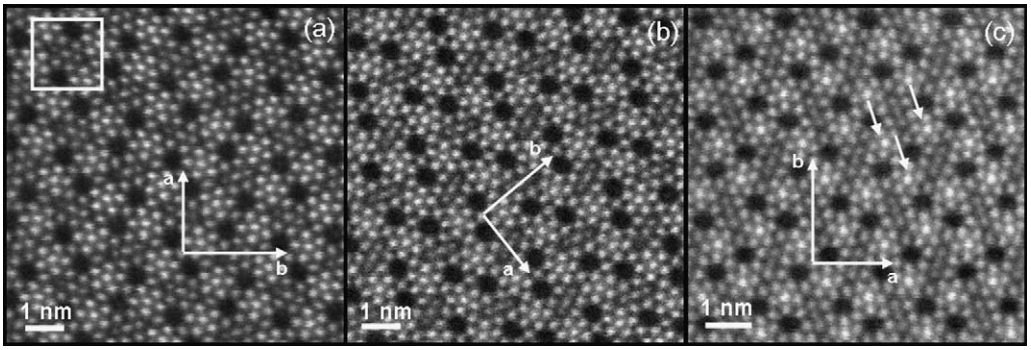

Fig. 2. HAADF image of (a) M1-Mo, (b) M1-Nb, and (c) M1-Ta looking down the [0 0 1] or [00$\bar{1}$] projections. The *a*–*b* axis vectors represent the edges of single unit cells in each case. Note the low contrast associated with the atoms in the filled hexagonal ring enclosed within the box in part (a) and the high contrast observed for the pentagonal centers indicated by the arrows in part (c). Note that the images shown have not been processed or altered in any way.

within the pentagonal octahedral sites remains fairly constant for each sample, reinforcing our normalization assumption. Qualitatively, in Fig. 2a, the hexagonal ring enclosed in the white box in the M1-Mo catalyst appears to be systematically lower in contrast than the equivalent features in the M1-Nb and the M1-Ta catalysts. This suggests that this sample may contain higher vanadium occupancy in these sites.

A second distinctive feature can be observed in Fig. 2c: the atomic columns in the pentagonal centers of the M1-Ta specimen (white arrows) display very high contrast compared to those in the M1-Nb and the M1-Mo catalysts. This result suggests that this site contains a higher concentration of Ta compared to the rest of the structure. This is a key result, since it confirms the preferential position of Ta in the pentagonal center, as reported on the basis of diffraction data by DeSanto et al. for the same Ta-containing M1 catalyst [8]. This also reinforces the proposed position of Ta by Yamazoe and Kihlborg in an earlier study where dilute Ta substitution was used as a structural stabilizer for single crystal studies of Mo_5O_{14} [8b]. Another implication of this result is that it implies that the location of Nb in the M1-Nb structure is indeed in the pentagonal center, as has been previously assumed, provided that an isomorphic substitution of Ta for Nb does occur as we expect.

3.2. Quantitative analysis of x,y coordinates

The fractional *x*,*y* coordinates for all three catalysts were directly measured from the HAADF images and are displayed in Fig. 3, along with those calculated from the Rietveld refinement of DeSanto et al. for the MoVNbTeO catalyst [7]. The *x*,*y* coordinates from the STEM images were consistent with each other and with the calculated coordinates derived from the Rietveld refinement model, with the exception of intercalation site, S13. In each of the three catalysts analyzed, the heptagonal channels were found to be vacant. A detailed comparison between the M1-Nb sample prepared hydrothermally and the MoVTeNbO sample prepared using the slurry method used in the Rietveld refinement study by DeSanto et al. can be found in Ref. [23], where it was shown using HAADF imaging that site S13 was partially occupied in the MoVTeNbO sample prepared using slurry techniques. The vacant heptagonal channels in the M1-Ta sample were not consistent with the Rietveld model for the same catalyst, but in that case the heptagonal channel occupancy was reported as questionable due to unreasonable metal–oxygen bond distances [8]. In all cases, the uncertainties in the measurements were small compared with the size of the symbols in Fig. 3, and the typical deviation was within the range of 0.05–0.15 Å.

For the measurement of the atomic coordinates, the method of using four points of reference, as discussed above, allowed for measurements that minimize the influence of rastering distortions. However, the symmetry requirements of the *Pba*2 space group dictate that site S1 must be located at (0,0) and site S2 must be at (0,0.5), since these are on the reference points. Therefore, the slight shifts in the relative positions of these two metal sites can be used to assess the magnitude of residual error/uncertainty from sample drift or rastering distortions not fully accounted for by the averaging. Making adjustments based on these symmetry-restricted points, the remaining contributions to the error in the fractional positions that can be attributed to the distortions are on the order of 0.10 Å (Fig. 3). Using this estimate as a benchmark for the random and systematic errors, any deviations in the fractional coordinates that are systematically much larger than 0.10 Å should be considered significant and suggest that an adjustment to the Rietveld model may be needed. However, the variations in the fractional coordinates for all metal sites are small, suggesting that *no revision* to the refined atomic coordinates reported by DeSanto et al. for both the MoVTeNbO [7] and the MoVTeTaO [8] Rietveld models is needed at this level of precision.

An important result is that the removal of Nb or the replacement of Nb with Ta does not have a significant effect on the coordinates of the framework metal sites. This suggests that the significant variations observed for the catalytic performance of the M1 catalyst are related to changes in the chemical composition of the catalytic surface, and structural strain or metal distance variations are unlikely to be responsible for variations in catalytic properties. However, this analysis does not take into account the influence of defects on the observed catalytic properties. We are currently analyzing both the influence of compositional variation and the effect of crystalline order and defects on the observed activity/selectivity as various elements are added or removed (e.g. Nb, Ta, Te, and Sb).

3.3. Quantitative analysis of occupancies

The contrast ratio for each site, referenced against the average pentagonal ring octahedral site contrast, was calculated for all three samples and is shown in Fig. 4a. The contrast results from analyses of the three samples were then compared with the expected contrast ratios as predicted from the Rietveld refinement models from both the MoVTeNbO [7] and MoVTeTaO [8] catalysts. Overall, the comparison of the M1-Mo and the M1-Nb contrast ratios, as measured directly from raw HAADF images, is largely consistent with the contrast ratios calculated from the refined M1 structural models [7]. The same is observed when comparing the

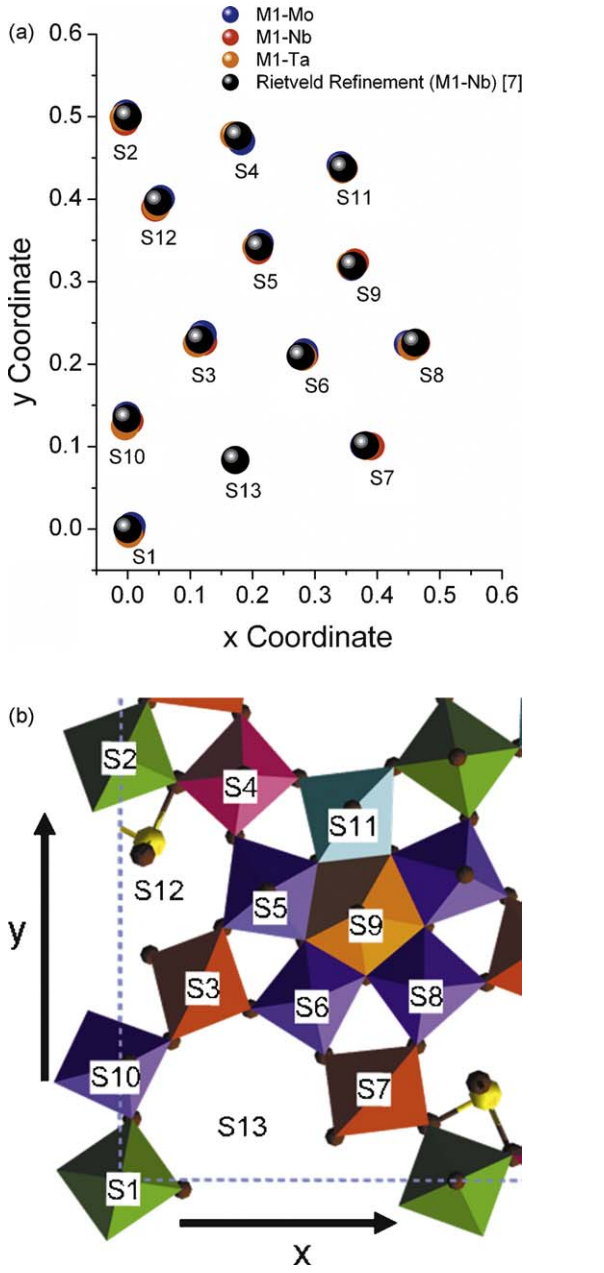

Fig. 3. Comparison of the fractional coordinates for each of the metal sites measured directly from HAADF images and the coordinates from the Rietveld refinement by DeSanto et al. [7]. The reference image shows the position of each metal site within one unit cell quadrant. In all three of the M1 catalysts studied, metal site 13 was vacant.

M1-Ta measurements with the refined MoVTeTaO contrast ratios [8]. In both cases, the sites that were predicted to have mixed occupancy displayed variable contrast compared to those expected to be pure Mo sites. For all samples, the Te composition in the S12 site from HAADF was significantly lower than expected from the Rietveld models. This apparent discrepancy was expected, however, since Te is highly volatile under TEM illumination [3]; previous experience using conventional bright-field high resolution TEM imaging of MoVTeNbO yielded images with completely vacant heptagonal and hexagonal channels due to beam-induced Te sublimation [7]. Some of the Te is retained under the gentler STEM operating conditions used in this study, but partial sublimation remains.

Close examination of the measurements for the sites with mixed occupancy (i.e. S1, S2, S3, S4, and S7) showed significant variations among the three catalyst samples, as shown in Fig. 4b. For sites S1, S4, and S7, there was a clear trend of decreasing V content with the substitution of Nb or Ta for Mo in the sequence: M1-Mo > M1-Nb > M1-Ta. For site S3, the trend order reverses for Nb and Ta samples: M1-Mo > M1-Ta > M1-Nb. Finally, the trend for vanadium content in site S2 follows the order: M1-Ta > M1-Nb > M1-Mo.

As reported in our previous HAADF papers [22,23], the V content attributed to site S4 based on HAADF contrast was in conflict with the full Mo occupancy indicated in the Rietveld models [7,8]. Although it could be argued that near-surface enrichment of vanadium could explain difference between HAADF results and diffraction results, we believe that a more likely explanation is that the occupancy of the S4 site may have been prematurely locked at full Mo occupancy in the course of the ~200-parameter Rietveld fitting process. Re-evaluation of these Rietveld data is in progress to test this. Looking back at the structural model in Fig. 1, it is reasonable to expect that site S4 would have similar occupancy to S7, due to geometric similarity; where site S7 shows ~30% V occupancy. Comparing the HAADF contrast for S4 with S7 supports the contention that these sites have similar occupancies. The observation of V in site S4 is also consistent with a recent Rietveld refinement of X-ray data from a hydrothermally prepared MoVTeNbO catalyst by Murayama et al. [16].

In comparing the Rietveld model for M1-Ta with HAADF results from multiple crystallites taken from the same specimen, we also note that the vanadium content of S3 and S7 is consistently lower from the HAADF analyses. The Rietveld refinement model showed 64% V in S3 and 41% V in S7 [8], as compared with 30% and 15%, respectively, based on HAADF contrast. As we will discuss in the next section, the M1-Ta specimen shows evidence of unmixing into Ta-rich and Ta-poor domains, therefore, the significance of the Rietveld-based bulk average model should be carefully interpreted in terms of the occupancies.

Based on our results, it appears that the overall vanadium content in the octahedral sites that link together the pentagonal rings decreases as the occupation of the S9 site by Nb or Ta increases. This may be a consequence of the electroneutrality constraint, since we are replacing Mo (Group VI) with a Group V element. The pattern of occupancies, however, is such that the decreased vanadium occupation overall does not arise from a simple linear decrease in each of the individual octahedral sites. The shifts in site preferences with S9 occupation seem to involve some additional chemical influences that have yet to be recognized.

3.3.1. *Phase segregation in the MoVTaTeO M1 system*

During the analysis of several different M1-Ta crystallites, ⟨0 0 1⟩ HAADF images revealed the presence of two distinct M1 phase compositions based on HAADF contrast analysis. Comparing ⟨0 0 1⟩ HAADF images from three crystallites (Fig. 5), it is apparent both visually and with quantitative contrast analysis that there exist Ta-rich and -poor domains or particles. Fig. 5(a) and (c) are typical of the Ta-rich phase with distinctively bright contrast for the pentagonal centers (site S9). Fig. 5b shows different contrast patterns, where the pentagonal centers *do not* show the high S9 contrast. Based on our limited sampling, it appears that the Ta-rich phase is dominant for this particular preparation. Quantitative contrast analysis is provided in Fig. 6 showing a comparison of the three particles from Fig. 5.

The contrast ratios measured for particles 1 and 3 are consistent with one another across all sites and indicate a consistent composition in those domains that exhibit bright contrast in the pentagonal centers. However, comparing with particle 2, several

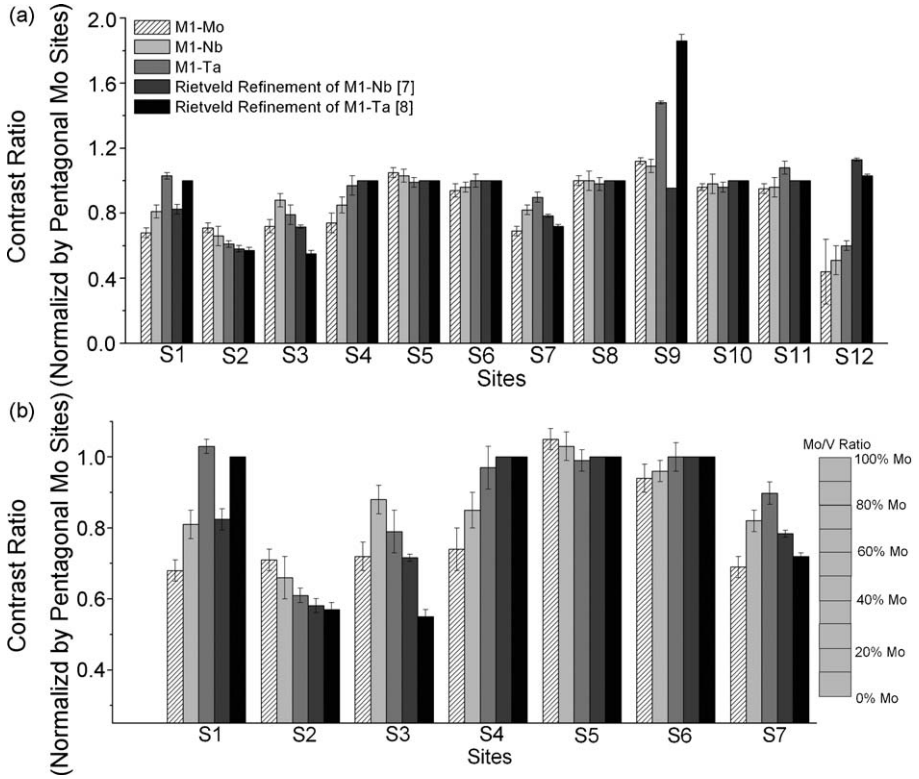

Fig. 4. (a) Comparison of the atomic column contrast ratios as a function of site position for M1-Mo, M1-Nb, M1-Ta, and the expected ratio based on the refined MoVTeNbO [7] and the MoVTeTaO [8] M1 structural models of DeSanto et al. (b) An expanded view of sites S1–S7 along with a scale bar showing relationship between the corresponding Mo/V occupancy and the contrast ratio. The legend applies to both part (a) and (b).

atomic sites show significant contrast variations. In addition to differences in the contrast levels for S9, major discrepancies are also found for sites S1 and S2, the two binary axis sites in the unit cell. For site S1, the Ta-rich domains show ~0% V occupancy, whereas the Ta-poor domains show ~25% V. For site S2, the Ta-rich domains show ~64% V and the Ta-poor domains show ~20% V. In both cases, the occupancies are somewhat different from the Rietveld model, with the Ta-rich domains giving closer agreement than the Ta-poor, consistent with the Ta-rich domains being dominant [7,8]. This phase coexistence phenomenon may indicate the presence of a miscibility gap. Likely differences in catalytic properties of preparations with homogeneous and heterogeneous Ta distribution have yet to be explored.

In exploring the domain structure of M1-Ta more carefully, we examined various regions around each of the particles to identify spatial patterns in the bright contrast S9 sites. Examples at various magnifications are displayed in Fig. 7. The HAADF image in Fig. 7a was taken from a position near the center of the same particle used in Fig. 6 (i.e. particle 2) and is reproduced from Fig. 5b for purposes of direct comparison. The image in Fig. 7b was obtained at near the edge of the same particle. Close examination shows evidence of high Ta concentrations in the S9 pentagonal centers since these sites exhibit high contrast compared to the same pentagonal positions in Fig. 7a. Estimates of the atomic contrast ratios from this edge region of particle 2 (not provided) are roughly consistent with those measured from particles 1 and 3 (Fig. 6). These results provide evidence of two distinct compositions that coexist within the same contiguous particle (i.e. coherently intergrown). The image in Fig. 7c, obtained from particle 2, shows an additional section of the particle edge exhibiting a mix of high and low

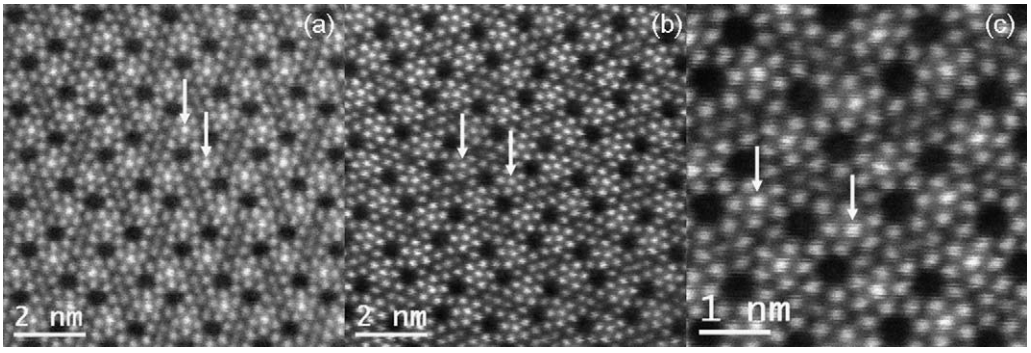

Fig. 5. (a) HAADF image showing a M1-Ta particle exhibiting enhanced contrast in the pentagonal centers. (b) HAADF image showing a different M1-Ta particle exhibiting diminished contrast in the pentagonal centers. (c) HAADF image showing a third M1-Ta particle exhibiting enhanced contrast in the pentagonal centers.

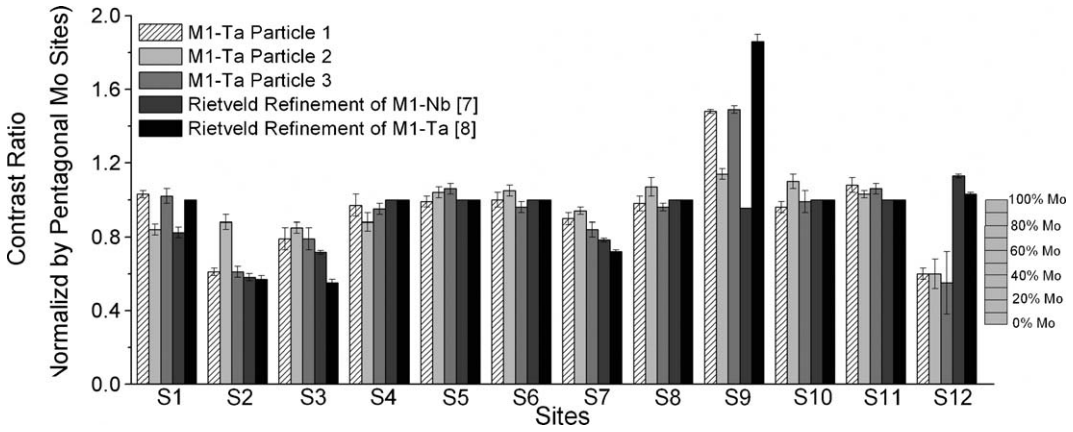

Fig. 6. Comparison of the atomic column contrast ratios as a function of site position for three different particles from the M1-Ta sample and the expected contrast ratio based on the refined MoVTeNbO [7] and the MoVTeTaO [8] M1 structural models of DeSanto et al.

contrast pentagonal centers (white versus red arrows). Local clustering of these high or low contrast S9 sites is consistent with phase separation rather than simple disorder, but no distinct domain walls are observed. This may simply indicate that the domain wall energies are low. The images in Fig. 7b and c also show that the Ta-rich domains of the multiphase particles are primarily found to be near the edges of the crystal, suggesting that the segregation may be influenced by either crystallite thickness or proximity to surfaces of the ⟨0 0 1⟩ zone. This might have important implications for the catalytic performance.

It is interesting to contemplate the likely possibility that there may also be Nb phase separation in the M1-Nb system, by analogy with the M1-Ta. There would be no easy way to detect this from diffraction data, and evidence from HAADF would have to be indirect in the form of bimodal vanadium occupancies in contiguous unit cells. This hypothesis is consistent with recent low energy ion scattering (LEIS) studies by Guliants et al. on the MoVTeNbO catalyst [12]. The results from the LEIS study indicated an enrichment of Nb of ∼55% at the surface of the M1 crystals compared to the bulk ICP results [12]. Since the M1 habit is typically that of long needles, this observation of surface enrichment of Ta towards the long lateral faces perpendicular to the *a*–*b* plane supports the claim of Guliants et al. for surface Nb-enrichment, since the bulk LEIS study would preferentially sample these same lateral faces. These lateral faces would constitute a large percentage of the exposed crystal facets in a sample with a needle-like morphology. However, further HAADF analysis of many M1 crystallites is required to better demonstrate and understand the occurrence of the Ta segregation behavior and to search for indirect evidence to support segregation of Nb-rich and -poor domains.

3.4. Structure–catalytic property relationships

The greatest challenge to development of a full understanding of the catalytic mechanism is in the isolation of the various factors that affect the observed catalytic performance. Some of these factors include the need for complex synthetic strategies that often lead to the coexistence of multiple complex phases, accurate identification/quantification of each individual phase, the degree of crystallinity, the particle morphology, and the solubility/location of each element within each phase. Due to these complexities, debate still exists over whether the catalysis occurs on well-organized and isolated active sites located on (0 0 1) faces [10,11] or if an amorphous overlayer is all that is required [47], since the (0 0 1) faces comprise only a very small fraction of the overall exposed surface due to the needle-like morphology.

In this work, we used aberration-corrected HAADF imaging to evaluate the chemical and structural changes that occur upon the substitution of Nb and Ta into the M1 framework. The results demonstrated that the addition of either of these elements does not change the positions of each atomic column, but does change the occupancies within these columns. Previous studies using phase-pure samples have shown that the addition of Nb to the M1

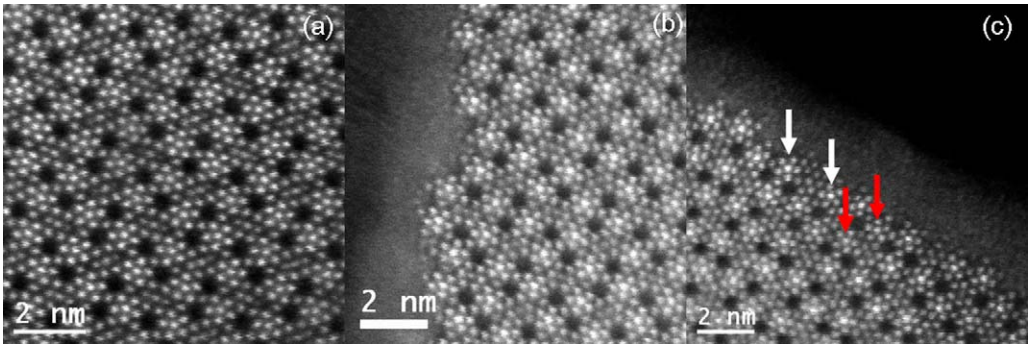

Fig. 7. (a) HAADF image showing the M1-Ta particle from Fig. 5 (particle 2) with the diminished contrast in the pentagonal centers. (b) HAADF image from the edge of the same particle showing a region of the particle at the edge of the crystal showing pentagonal centers with enhanced contrast. (c) A second HAADF image of the edge of the same particle as part (a) and (b) showing some pentagonal centers with enhanced contrast (white arrows), and others nearby with diminished contrast (red arrows). In both (b) and (c), the bright pentagonal centers indicate possible Ta segregation to the crystal surfaces perpendicular to the ⟨0 0 1⟩ direction of the M1-Ta crystallite. (For interpretation of the references to color in this figure legend, the reader is referred to the web version of the article.)

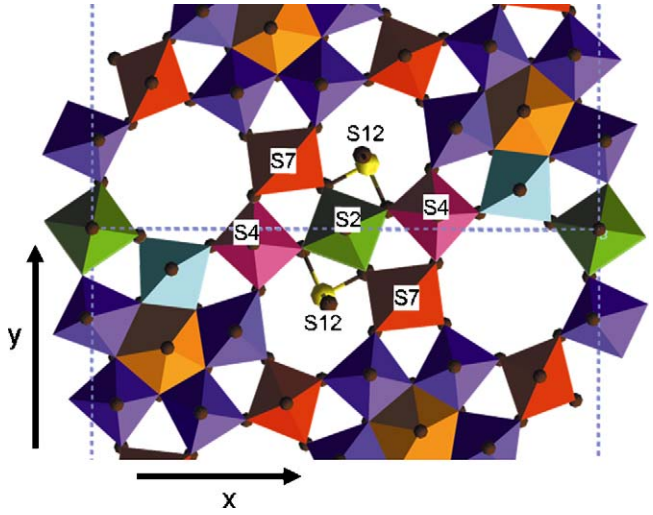

Fig. 8. Rendering of the M1 framework highlighting the proposed M1 active site [11].

catalyst provides a ~20% increase in the selectivity of acrylonitrile [38]. A second study using phase-pure M1 demonstrated that the substitution of Ta into the framework produced a catalyst with comparable acrylonitrile yields to those from the Nb-substituted M1 catalysts [10].

Using the site isolation model and assuming that catalysis occurs on an organized active site as depicted in Fig. 8a [11], we can use the measured occupancies from the HAADF images to calculate the expected distribution of Mo and V throughout the active site for each of the three specimens. This analysis differs from the probability model proposed by Grasselli et al. [11] in that we have shown in this study, and in our previous HAADF studies, that site S4 can contain significant amounts of V, comparable to site S7 [22,23]. Measured occupancies within the active site (i.e. S2, S4, and S7) are listed in Table 2 and associated probabilities for the active site containing between zero and five V atoms are provided in Table 3. The results show that ~86% of M1-Nb and ~97% M1-Ta will have an active site that is composed of less than three V atoms, whereas the M1-Mo specimen will have ~64% of the active sites containing less than three V atoms. The increasing V concentration within the active site corresponds with the decreasing trend in selectivity when comparing the M1-Mo specimen to the Ta- and Nb-substituted phases. This trend is consistent with the proposed active site of Grasselli et al. where they suggested that a site with more than one V^{5+} will lead to combustion, one V^{5+} leads to an active and selective site, and no V^{5+} would lead to an inactive site [11]. In this case, the calculated number of V atoms will be higher, since we incorporate the increased V occupancy of site S4. The role of Nb and Ta in these catalysts appears to be a V director, where the choice of pentagonal biprismatic substitution element controls the distribution of V occupancies in the linking octahedral sites. Therefore, it appears that an optimal V occupancy can be achieved with controlled pentagonal biprismatic substitution, where the proper balance between V^{5+} and V^{4+} is tuned such that maximum selectivity towards acrylonitrile/acrylic acid is accomplished. It is also important to note that the current analysis ignores the role of M2 as a promoter phase, possible defect correlations, the effect of statistical Te occupancy (partial occupancy at the active site), the inhomogeneous distribution of Ta (and possibly Nb) within the M1 crystallites, and shifts in the vanadium valence. We are currently in the process of investigating several of these factors.

Table 2
The Mo and V occupancies measured from HAADF images for the active site (S2, S4, S7) from the M1-Mo, M1-Nb, and M1-Ta (Ta-rich domain) catalysts.

Measured occupancy of molybdenum and vanadium in the active site						
Site #	M1-Mo		M1-Nb		M1-Ta	
	Mo (%)	V (%)	Mo (%)	V (%)	Mo (%)	V (%)
S2	57	43	50	50	42	58
S4	62	38	79	21	95	5
S7	53	47	74	26	85	15

Table 3
The calculated probability that an active site within the M1-Mo, M1-Nb, or M1-Ta (Ta-rich domain) catalyst will contain between zero and five vanadium atoms.

Probability of vanadium occupancy in the active site			
# of V atoms in the active site	M1-Mo (%)	M1-Nb (%)	M1-Ta (%)
0	6	17	27
1	23	38	50
2	34	31	19
3	26	12	3
4	9	2	0
5	1	0	0

4. Conclusions

In this work, we performed a systematic study of the effect of substituting or removing Group V elements into the M1 framework structure. The results of this study demonstrate the following. (1) The positions of the M1 framework atomic columns are, to a first approximation, independent of chemical variations to within the precision of the HAADF analysis (~0.1 Å). Furthermore, these coordinates are in agreement with the Rietveld models of DeSanto et al. for both MoVTeNbO [7] and MoVTeTaO [8] to within experimental error. (2) Aberration-corrected HAADF imaging is sensitive to the local compositional variations in the atomic columns through analysis of *Z*-contrast variations, which can be quantified using the approximate relationship between the observed contrast and the square of the atomic number *Z*. (3) The addition/removal of Nb or the replacement of Nb with Ta induces significant changes in the elemental occupancies in the framework. (4) The M1-Ta system appears to contain two chemical compositions, indicative of some form of phase unmixing, and this may also indicate likely phase separation in M1-Nb. (5) In the case of the M1-Ta crystallite with local composition heterogeneity, Ta appears to preferentially segregate to the edges of the *a*–*b* plane. (6) The addition of Nb or Ta to the M1 framework leads to a significant change in the V distribution among the octahedral sites that link the pentagonal units and are considered the active site. The trends in vanadium content within the proposed active site are consistent with the statistical analysis reported earlier [11] except that adjustment for vanadium occupancy in site S4 perturbs the proposed requirements for active, inactive, and combustion sites. Further analysis is needed to develop distinct trends relating the V content in the active site and catalytic performance.

The existing M1/M2 literature is comprised of a wide variety of studies focused on both characterization and catalytic evaluation using a multitude of different formulations. In this work, and several reports to follow, we employ high-resolution HAADF studies that allow us to systematically probe, atom column by atom column, the changes in both the framework positions and composition. The goal of these studies is to develop a library of relationships that describe the structural and chemical changes that occur upon the addition, removal, or substitution of frame-

work elements in the M1 system. In this study, we have initiated assembly of this library for the effects of Group V elements on the M1 framework. As our future studies expand to include other M1 combinations, our hope its to compare our library of chemical information to the existing wealth of catalytic studies available in the literature, with the goal of developing structure–catalytic performance relationships that allow an improved understanding of the underlying mechanism for selective oxidation over the M1 catalyst, and to identify clues to further improve the M1 catalyst for various selective oxidation reactions.

Acknowledgments

We acknowledge Claus G. Lugmair and Anthony F. Volpe Jr. of Symyx Technologies, Inc., for providing some of the M1 specimens used in this study. V.V. Guliants acknowledges the financial support from the Chemical Sciences, Geosciences and Biosciences Division, Offices of Basic Energy Sciences, Office of Science, U.S. Department of Energy under Grant No. DE-FG02-04ER15604. D. Blom and T. Vogt thank the State of South Carolina and the Vice President of Research & Health Sciences at the University of South Carolina for generous support.

References

[1] J.N. Al-Saeedi, V. Vasudevan, V.V. Guliants, Catal. Commun. 4 (2003) 537.
[2] M. Aouine, J.L. Dubois, J.M.M. Millet, Chem. Commun. (2001) 1180.
[3] M. Baca, M. Aouine, J.L. Dubois, J.M.M. Millet, J. Catal. 233 (2005) 234.
[4] M. Baca, J.M.M. Millet, Appl. Catal. A 288 (2005) 243.
[5] P. Botella, P. Concepcion, J.M. Lopez Nieto, Y. Moreno, Catal. Today 99 (2005) 51.
[6] P. DeSanto, D.J. Buttrey, R.K. Grasselli, C.G. Lugmair, A.F. Volpe, B.H. Toby, T. Vogt, Top. Catal. 23 (2003) 23.
[7] P. DeSanto, D.J. Buttrey, R.K. Grasselli, C.G. Lugmair, A.F. Volpe, B.H. Toby, T. Vogt, Z. Fur Kristallogr. 219 (2004) 152.
[8] (a) P. DeSanto, D.J. Buttrey, R.K. Grasselli, W.D. Pyrz, C.G. Lugmair, A.F. Volpe, T. Vogt, B.H. Toby, Top. Catal. 38 (2006) 31;
(b) N. Yamazoe, L. Kihlborg, Acta Crystallogr., Sect. B: Struct. Sci. 31 (1975) 1666.
[9] R.K. Grasselli, Catal. Today 99 (2005) 23.
[10] R.K. Grasselli, D.J. Buttrey, J.D. Burrington, A. Andersson, J. Holmberg, W. Ueda, J. Kubo, C.G. Lugmair, A.F. Volpe, Top. Catal. 38 (2006) 7.
[11] R.K. Grasselli, D.J. Buttrey, P. DeSanto, J.D. Burrington, C.G. Lugmair, A.F. Volpe, T. Weingand, Catal. Today 91–92 (2004) 251.
[12] V.V. Guliants, H.H. Brongersma, A. Knoester, A.M. Gaffney, S. Han, Top. Catal. 38 (2006) 41.
[13] J. Holmberg, R.K. Grasselli, A. Andersson, Top. Catal. 23 (2003) 55.
[14] J. Holmberg, R.K. Grasselli, A. Andersson, Appl. Catal. A 270 (2004) 121.
[15] J.M. Lopez Nieto, P. Botella, B. Solsona, J.M. Oliver, Catal. Today 81 (2003) 87.
[16] H. Murayama, D. Vitry, W. Ueda, G. Fuchs, M. Anne, J.L. Dubois, Appl. Catal. A 318 (2007) 137.
[17] T. Ushikubo, H. Nakamura, Y. Koyasu, S. Wajiki, US Patent 5,380,933 (1995).
[18] T. Ushikubo, H. Nakamura, Y. Koyasu, S. Wajiki, EP Patent 608 838 B1 (1997).
[19] W. Ueda, D. Vitry, T. Katou, Catal. Today 96 (2004) 235.
[20] T. Ushikubo, K. Oshima, A. Kayou, M. Vaarkamp, M. Hatano, J. Catal. 169 (1997) 394.
[21] D. Vitry, Y. Morikawa, J.L. Dubois, W. Ueda, Appl. Catal. A 251 (2003) 411.
[22] W.D. Pyrz, D.A. Blom, T. Vogt, D.J. Buttrey, Angew. Chem., Int. Ed. 47 (2008) 2788.
[23] W.D. Pyrz, D.A. Blom, N.R. Shiju, V.V. Guliants, T. Vogt, D.J. Buttrey, J. Phys. Chem. C 112 (2008) 10043.
[24] J.N. Al-Saeedi, V.V. Guliants, Appl. Catal. A 237 (2002) 111.
[25] T. Blasco, P. Botella, P. Concepcion, J.M.L. Nieto, A. Martinez-Arias, C. Prieto, J. Catal. 228 (2004) 362.
[26] P. Botella, A. Dejoz, J.M.L. Nieto, P. Concepcion, M.I. Vazquez, Appl. Catal. A 298 (2006) 16.
[27] R.M. Feng, X.J. Yang, W.J. Ji, H.Y. Zhu, X.D. Gu, Y. Chen, S. Han, H. Hibst, J. Mol. Catal. A: Chem. 267 (2007) 245.
[28] R.K. Grasselli, J.D. Burrington, D.J. Buttrey, P. DeSanto, C.G. Lugmair, A.F. Volpe, T. Weingand, Top. Catal. 23 (2003) 5.
[29] M.O. Guerrero-Perez, J.N. Al-Saeedi, V.V. Guliants, M.A. Banares, Appl. Catal. A 260 (2004) 93.
[30] V.V. Guliants, R. Bhandari, B. Swaminathan, V.K. Vasudevan, H.H. Brongersma, A. Knoester, A.M. Gaffney, S. Han, J. Phys. Chem. B 109 (2005) 24046.
[31] H. Hibst, F. Rosowski, G. Cox, Catal. Today 117 (2006) 234.
[32] Y. Li, S. Bhatt, G. Beaucage, V.V. Guliants, S. Mamedov, R.S. Soman, J. Phys. Chem. B 109 (2005) 23250.
[33] J.M.M. Millet, M. Baca, A. Pigamo, D. Vitry, W. Ueda, J.L. Dubois, Appl. Catal. A 244 (2003) 359.
[34] O.V. Safonova, B. Deniau, J.M.M. Millet, J. Phys. Chem. B 110 (2006) 23962.
[35] W. Ueda, K. Oshihara, Appl. Catal. A 200 (2000) 135.
[36] W. Ueda, D. Vitry, T. Kato, N. Watanabe, Y. Endo, Res. Chem. Intermed. 32 (2006) 217.
[37] W. Ueda, D. Vitry, T. Katou, Catal. Today 99 (2005) 43.
[38] N. Watanabe, W. Ueda, Ind. Eng. Chem. Res. 45 (2006) 607.
[39] V.V. Guliants, R. Bhandari, A.R. Hughett, S. Bhatt, B.D. Schuler, H.H. Brongersma, A. Knoester, A.M. Gaffney, S. Han, J. Phys. Chem. B 110 (2006) 6129.
[40] H. Hibst, A. Tenten, L. Marosi, BASF Aktiengesellschaft, Patent EP 774 297 Publ. 21.06, 1997.
[41] P.E. Batson, N. Dellby, O.L. Krivanek, Nature 418 (2002) 617.
[42] Z. Liu, K. Suenaga, S. Iijima, J. Am. Chem. Soc. 129 (2007) 6666.
[43] Neutron scattering cross-sections obtained from the NIST Center for Neutron Research webpage: http://www.ncnr.nist.gov/resources/n-lengths/list.html on May 27, 2008.
[44] T. Hahn (Ed.), International Tables for Crystallography, vol. A, D, Reidel Publishing Company, Dordrecht, 1983, p. 223.
[45] E. Abe, S.J. Pennycook, A.P. Tsai, Nature 421 (2003) 347.
[46] A. Howie, J. Microsc. (Oxford) 117 (1979) 11.
[47] J.B. Wagner, O. Timpe, F.A. Hamid, A. Trunschke, U. Wild, D.S. Su, R.K. Widi, S.B. Abd Hamid, R. Schlogl, Top. Catal. 38 (2006) 51.
[48] P. Korovchenko, N.R. Shiju, A.K. Dozier, U.M. Graham, M.O. Guerrero-Pérez, V.V. Guliants, Top. Catal. 50 (2008) 43.